Journal of Porphyrins and Phthalocyanines
J. Porphyrins Phthalocyanines 2019; **23**: 1–10
DOI: 10.1142/S1088424619501001

Published at http://www.worldscinet.com/jpp/

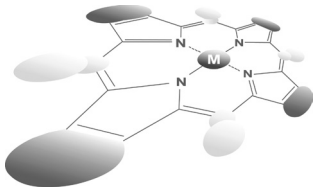

Tropylium cation-fused aromatic [26]dicarbaporphyrinoids with NIR absorptions: Synthesis, spectroscopic and theoretical characterization

Krushna C. Sahoo[a], Mohandas Sangeetha[b], Dandamudi Usharani*[b,c] and Harapriya Rath*[a]

[a]*School of Chemical Sciences, Indian Association for the Cultivation of Science, 2A/2B Raja SC Mullick Road, Jadavpur, Kolkata 700032, India*
[b]*Department of Food Safety and Analytical Quality Control Laboratory, CSIR-Central Food Technological Research Institute, Mysuru, Karnataka, 700020, India*
[c]*Academy of Scientific and Innovative Research (AcSIR), CSIR-HRDG, Gazhiabad, Uttarpradesh, India*

Dedicated to Professor Atsuhiro Osuka on the occasion of his 65th birthday.

Received 3 June 2019
Accepted 17 July 2019

ABSTRACT: An easy and efficient synthetic methodology for two hitherto unknown tropylium-cation-fused Hückel aromatic [26] dicarbaporphyrinoids has been developed by acid-catalyzed Lindsey type condensation of bithiophene/biselenophene diol with azulene using $BF_3 \cdot Et_2O$ followed by oxidation with chloranil and/or DDQ. Both the macrocycles have been achieved in moderately good yields. Their structures, aromaticity and optical properties have been elucidated by NMR, UV-vis-NIR spectroscopic analyses and in-depth theoretical calculations. Both the macrocycles exhibited strongly diatropic characteristics with the UV-vis spectra closely resembling the spectra for true porphyrins. Detailed structural analyses using ^1H–^1H COSY, ROESY and DFT level theoretical investigations indicated fully conjugated [26]π main conjugation pathway being benefitted by the tropylium character of the seven membered rings.

KEYWORDS: Hückel topology, core modification, carbaporphyrinoids, aromaticity, NIR absorption, DFT calculations.

INTRODUCTION

The ever-expanding applications in biological and opto-electronical fields such as photodynamic therapy agents, solar energy conversion materials, materials for nano-molecular devices, and nonlinear optical materials has urged synthetic chemists to exploit more and more efficient methodologies for synthesis of functionalized porphyrins. In such endeavors, π-system extension of porphyrins offers the possibility of shifting the major UV-vis absorptions to longer wavelengths, a particularly valuable feature that could have wide range of applications [1]. Designing such NIR-absorbing and/or emitting systems is of considerable interest due to their immense biomedical applications such as tissue diagnostics, photodynamic therapy dyes and microscopic imaging agents [2]. Very recently we reported the first ever aromatic [30] heteroannulenes with strong NIR absorption that have been well benefitted from the presence of intriguing resonance hybrid structures having rigid ethynylene-cumulene moieties (C_{sp} ═ C_{sp}) [3]. An alternative strategy to arrive at NIR absorptive dyes is ring fusion on the porphyrin ring. To gain more insights into the effects due to ring fusion on the porphyrin ring, many efforts have been made toward the

*Correspondence to: Dr. Harapriya Rath, tel.: +9133-2473-4971, fax: +9133-2473-2805, email: ichr@iacs.res.in; Dr. Dandamudi Usharani, tel.: +91821-251-4972, e-mail: ushad@cftri.res.in.

synthesis of π-extended porphyrins in the last decade [4]. Among the π-extended porphyrinoids, linearly fused aromatic rings exhibited significant advantages on the red-shifting effect although due to the extreme instabilities of pyrroles bearing linearly-fused acenes such as benzene, naphthalene and anthracene, synthesis of the acene-fused porphyrins still required expedient tactics [5]. Nevertheless, it still remains a challenge to conveniently enlarge the conjugated system and introduce versatile functional groups on the periphery for applications in different fields. Another way of altering the cavity size and perturbing electronic structure of the macrocycles is replacement of carbon(s) in place of pyrrole nitrogen(s), the so called Carbaporphyrins [6]. In common with N-confused porphyrins [7], these compounds have a CNNN core that can facilitate the generation of organometallic derivatives [8]. For instance, benzocarbaporphyrins and tropiporphyrins with indene or cycloheptatriene units in place of a pyrrole ring readily form silver (III) complexes and some gold (III) derivatives [9].

Among all the known carbaporphyrins, introduction of an azulene moiety to the porphyrinoid framework (Chart 1) is of particular interest because of the unusual electronic properties of this bicyclic system [10]. Synthesis of azuliporphyrin and its heteroanalogues have been found to exhibit borderline macrocyclic aromaticity from dipolar canonical forms that simultaneously give the structure carbaporphyrin and tropylium aromatic characteristics [11]. A perusal of the literature reveals the non-aromatic features of dithia- and dioxa-diazuliporphyrins which are easily oxidizable to their radical cations and consequently to aromatic dications [12]. It must also be emphasized that azuliporphyrins afford Ni (II), Pd (II) and Pt (II) complexes in addition to stable iridium (III) and rhodium (III) derivatives [13]. It is worth mentioning that even though core-modified ring-expanded heteroannulenes have been extensively studied because of their suitability for various applications [14], inclusion of azulene moieties in ring-expanded heteroannulenes has remained hitherto unexplored. The combination of azulene π systems with porphyrin macrocyclic frameworks leading to redox switchable materials along with fascinating metal complexes has thus inspired us to check the viability in expanded porphyrins and hence the undertaking of the work has been presented in this manuscript.

RESULTS AND DISCUSSION

Synthesis of the desired macrocycles is based on the fact that azulene favors electrophilic substitution in 1 and 3 positions that are structurally analogous to the α-positions in pyrrole. Using Lindsey type [3] condensation, a 1:1 molar ratio of azulene and bithiophene diol were stirred in dichloromethane under dilute conditions using $BF_3 \cdot Et_2O$ as a catalyst followed by oxidation with DDQ. Column chromatographic separation over basic alumina followed by repeated silica gel (200–400 mesh) chromatographic separation and preparative thin layer chromatography (PTLC) yielded 8% of extra pure macrocycle $[\mathbf{9}]^{2+}$ as green solid while macrocycle $[\mathbf{10}]^{2+}$ was obtained as green solid in 10% yield. Macrocycles $[\mathbf{9}]^{2+}$ and $[\mathbf{10}]^{2+}$, to the best of our knowledge are the first of the kind to have a 26π macrocyclic conjugation pathway in an expanded dicarbaporphyrinoid. Here, it is worthy to mention that, as proposed by Latos-Grażyński and co-workers

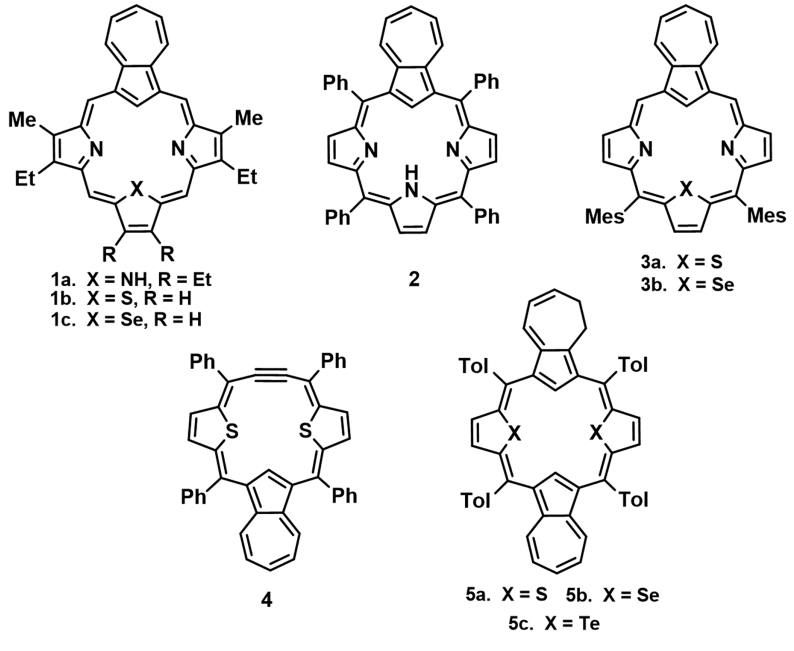

Chart 1. Representative structures of azulene-incorporated porphyrinoids

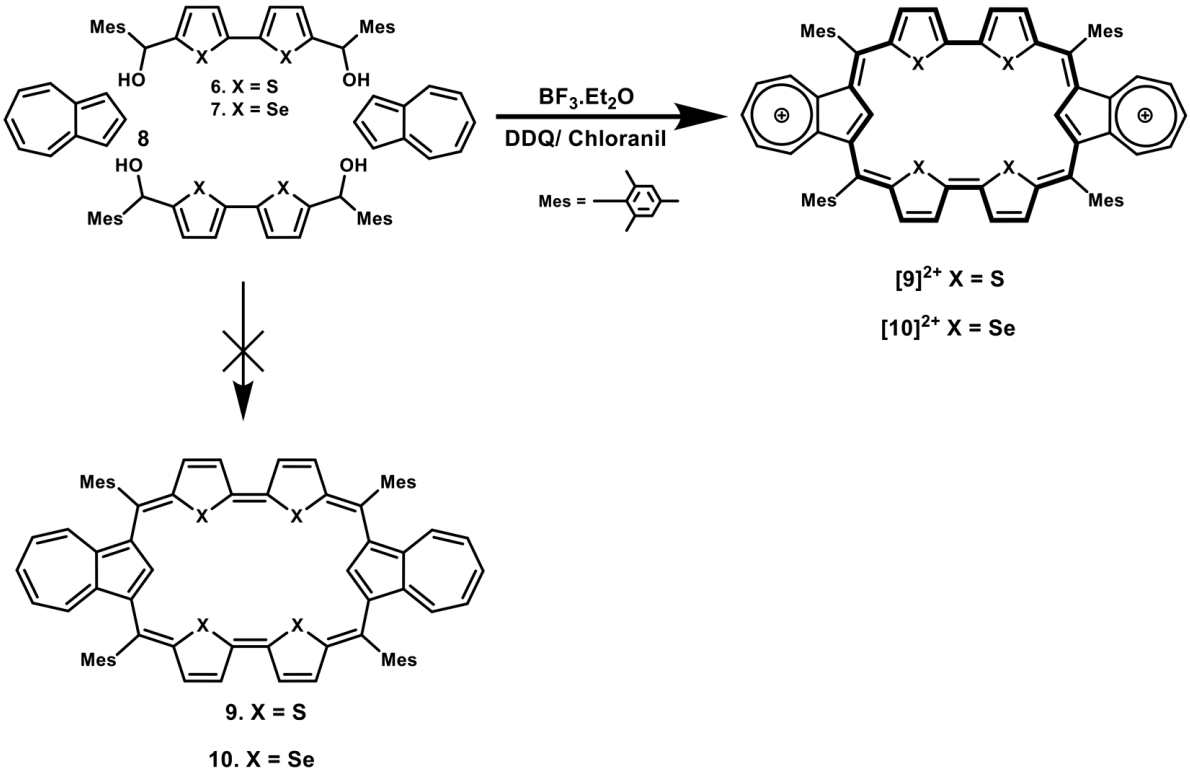

Scheme 1. Synthesis of macrocycles $[\mathbf{9}]^{2+}$ and $[\mathbf{10}]^{2+}$

where controlled addition of oxidant and/or reductant led to redox switchable chromophore, in our case using a mild oxidant or a strong oxidant in excess amount or stoichiometric amount led to formation of $[\mathbf{9}]^{2+}$ and $[\mathbf{10}]^{2+}$. We strongly believe that, unlike the lower congeners reported by Latos-Grażyński, neither neutral forms **9** and **10** nor the intermediate cation radical is stable enough to be isolated for both macrocycles $[\mathbf{9}]^{2+}$ and $[\mathbf{10}]^{2+}$.

Both macrocycles $[\mathbf{9}]^{2+}$ and $[\mathbf{10}]^{2+}$ described above were characterized by MALDI-TOF mass, UV-vis-NIR, ^{1}H and 2D NMR spectroscopy and in-depth theoretical calculations at the DFT level. MALDI-TOF mass analyses confirmed the proposed compositions for the macrocycles.

The presence of two azulene rings introduces an element of cross-conjugation that would be expected to disrupt macrocyclic aromaticity. However, for macrocycle $[\mathbf{9}]^{2+}$, a Soret like absorption at 587 nm and weak Q-band-like absorptions at 702 and 788 nm followed by a broad absorption band at 1305 nm has been observed, while the electronic absorption spectrum of $[\mathbf{10}]^{2+}$ is indeed extremely similar in shape and structure to the spectrum of $[\mathbf{9}]^{2+}$ exhibiting a Soret like absorption at 620 nm and weak Q-band-like absorptions at 735 and 802 nm followed by a broad absorption band at 1385 nm. The ε value for the Soret type band is on the order of 10^5 $M^{-1}cm^{-1}$ for both the macrocycles (Fig. 1). These observations from the electronic absorption spectra confer porphyrinic nature with aromaticity for both the macrocycles [15]. Also the effect of heteroatom substitution (S/Se) is realized through the red shift of the absorptions in the visible region and NIR region of the electromagnetic spectrum for $[\mathbf{10}]^{2+}$ compared to $[\mathbf{9}]^{2+}$.

In order to account for the isolated macrocycles not being the neutral forms **9/10**, DFT-level geometry optimization has been carried out for a thorough understanding of the electronic structures of **9/10** at the B3LYP/6-31G (*d*, *p*) level of theory (B1) using the Gaussian 16 program [16]. In-depth theoretical calculations on various isomers of **9** and **10** indicated that tetrathiophene or tetraselenophene are more stable in non-inverted forms (Fig. 2). An increase in the number of inverted thiophene rings further reduced the stability of the macrocyclic ring due to repulsion of inner CH's of thiophene with the inner CH's of the azulene rings (Figs S10–S11). The close inspection of geometric structure of the most stable isomer of **9** indicated the local aromatic nature of the azulene moieties. It is worthy to note that the C_α–C_β and C_β–C_β distances for thiophene rings and C–C bond lengths of the azulene rings are very similar to reported crystal structures of **5**a and **5**b [12] and the C_α–C_α bond distance of the bithiophene ring is close to the original tetrathia rubyrin [14c]. While the azulene rings are out of the plane where mean plane deviation with respect to *meso* carbons of macrocycle is 42.5° and 41.5° for **9** and **10**. Moreover, in order to gain insight into the electronic absorption spectral patterns of **9** and **10**, we performed TD-DFT calculations at the B1 level

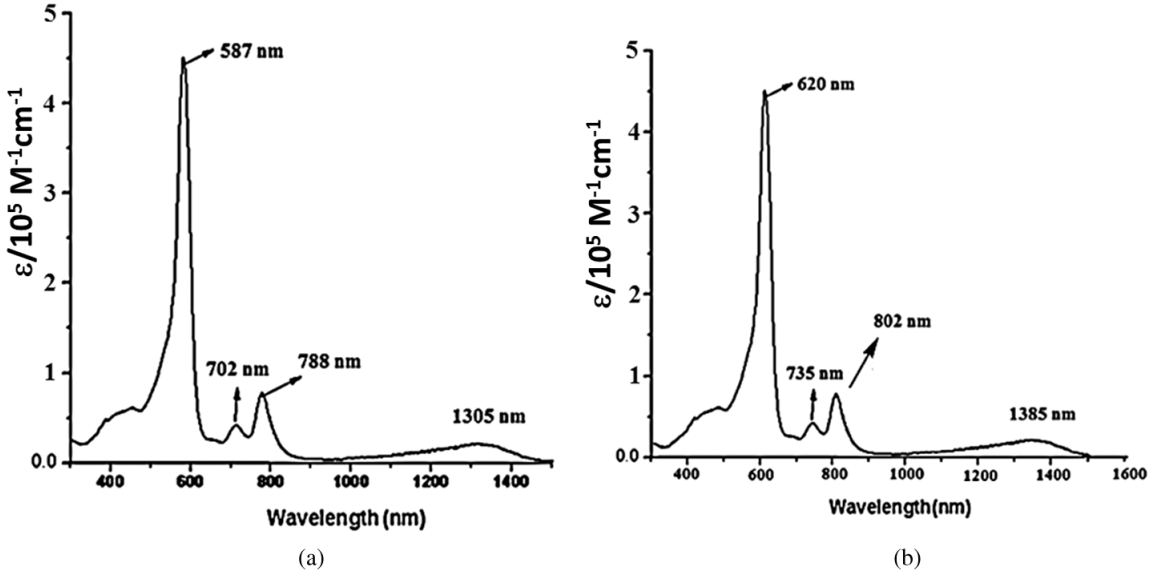

Fig. 1. UV-vis-NIR absorption spectra of macrocycles (a) $[\mathbf{9}]^{2+}$ and (b) $[\mathbf{10}]^{2+}$ in dichloromethane

of theory [17]. The simulated UV-vis spectra in presence of dichloromethane for **9** and **10** did not show any NIR absorption bands (Figs S12–S15) as we observed in the steady-state absorption spectra (Fig. 1) of our isolated macrocycles. To gain deeper insight into the aromaticity of **9** and **10**, we conducted Nucleus-Independent Chemical shift (NICS) [18] calculation. The NICS(0) values at the center of the macrocycles were estimated to be 2.22 and 2.21 ppm respectively (Fig. S16), indicating the meager antiaromatic character. Additionally, the localized aromatic character of the azulene and thiophene rings (Fig. S17) has been clearly illustrated by Anisotropy of the Induced Current Density (ACID) plots [19] which seems to be in line with the proposed conjugated pathway observed in neutral forms of **5**a and **5**b [12]. Further investigation of inverted thiophene conformations for both **9**a and **10**a also convinced us of the apparent nonaromaticity of macrocycles.

For an interpretation of the observed steady state electronic absorption spectra, one is urged to invoke π-electron delocalization motif with the isolated macrocycles being $[\mathbf{9}]^{2+}$ and $[\mathbf{10}]^{2+}$. These can have greater degree of combined carbaporphyrin and tropylium character as shown in Scheme 2, leading to charge delocalization rather than charge separation and hence accounting for the porphyrinic nature with aromaticity as inferred from electronic absorption spectrum (Fig. 1). Therefore, we carried out theoretical calculations to understand the most stable isomer of the macrocycles $[\mathbf{9}]^{2+}$ and $[\mathbf{10}]^{2+}$. Figure 3 summarizes DFT optimized geometry of the most stable conformer of $[\mathbf{9}]^{2+}$. Figure S19 summarizes all plausible conformers of $[\mathbf{9}]^{2+}$. It is to be noted that for the most stable conformer of $[\mathbf{9}]^{2+}$ the C–C bond lengths of the tropylium ring are delocalized (1.395–1.398Å), more like a tropylium cation. Moreover, in the optimized geometry of the most stable conformer of $[\mathbf{9}]^{2+}$, the delocalization of both the bithiophene rings is extended through the carbocyclic rings thereby leading to a 26π electron conjugation pathway as depicted in the Scheme 2. The simulated UV-vis spectra (Fig. 4) in the presence of dichloromethane for $[\mathbf{9}]^{2+}$ and $[\mathbf{10}]^{2+}$ were found to coincide with the steady-state absorption spectra. On the basis of calculations, it has been envisaged that the strong Soret-like band and very weak Q-type bands observed in the steady state electronic absorption spectra of $[\mathbf{9}]^{2+}$ and $[\mathbf{10}]^{2+}$ mainly involve HOMO-1, HOMO, LUMO and LUMO+1 orbital transitions (Table S9–S10). The broad bands at 1305 nm and 1385 nm are a consequence of electronic vertical transition of HOMO and LUMO orbitals. The nature of HOMO and LUMO orbitals of $[\mathbf{9}]^{2+}$ and $[\mathbf{10}]^{2+}$ clearly indicate an extended π delocalization of the bithiophene ring with carbaporphyrin leading to lower HOMO–LUMO energy and the characteristic NIR absorption bands as observed in other expanded porphyrins [3, 14c]. In contrast to the frontier orbitals of expanded carbaporphyrinoids $[\mathbf{9}]^{2+}$ (Fig. 4), the nature of LUMO orbitals of **5**a are azulene π* orbitals (Fig. S25a).

Further evidence of the aromaticity of $[\mathbf{9}]^{2+}$ and $[\mathbf{10}]^{2+}$ has been elucidated through NICS(0) values at the center of the macrocycles which were found to be -8.54 ppm and -9.38 ppm respectively, indicating aromatic character. Figure 5 clearly depicts distinct clockwise ring currents in the AICD plots of $[\mathbf{9}]^{2+}$ and $[\mathbf{10}]^{2+}$, supporting the macrocyclic aromaticity. Furthermore, the estimated Harmonic Oscillator Model of Aromaticity (HOMA) [20] values of 0.860, 0.801 for $[\mathbf{9}]^{2+}$ and $[\mathbf{10}]^{2+}$ and degenerate frontier molecular orbital (FMOs) with energy level diagrams (Fig. S23) are well matched with their aromatic nature.

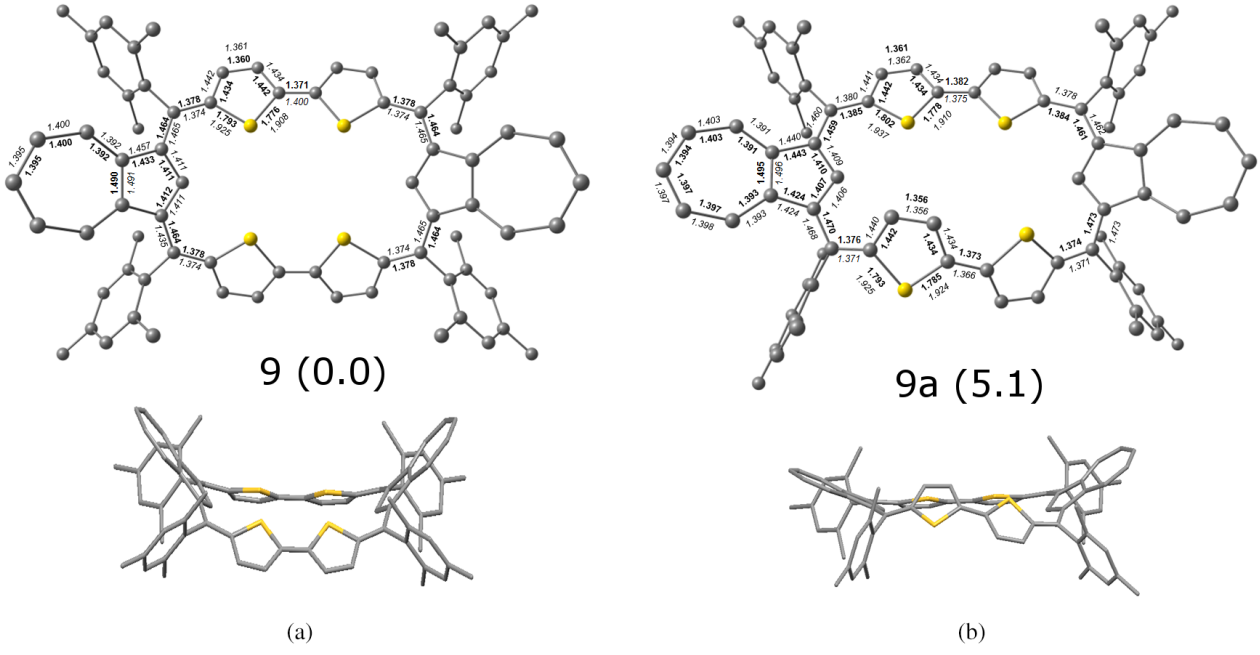

Fig. 2. Structural parameters of optimized geometries (a) **9** and (b) **9a** conformers in front and side view at B3LYP/6-31G(*d*, *p*) level of theory. Note that key bond length (Å) parameters are given for **9** in bold and for **10** in italics. Relative free energies (kcal/mol) are given in parenthesis. Hydrogen atoms are omitted for clarity sake

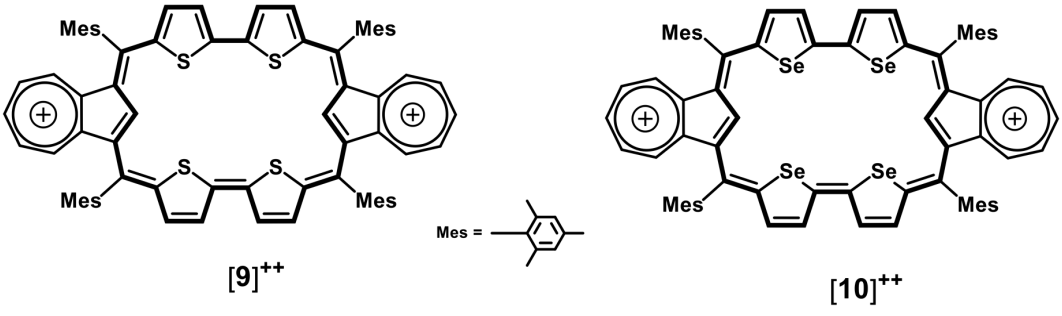

Scheme 2. 26π Conjugation pathway for macrocycles $[\mathbf{9}]^{2+}$ and $[\mathbf{10}]^{2+}$

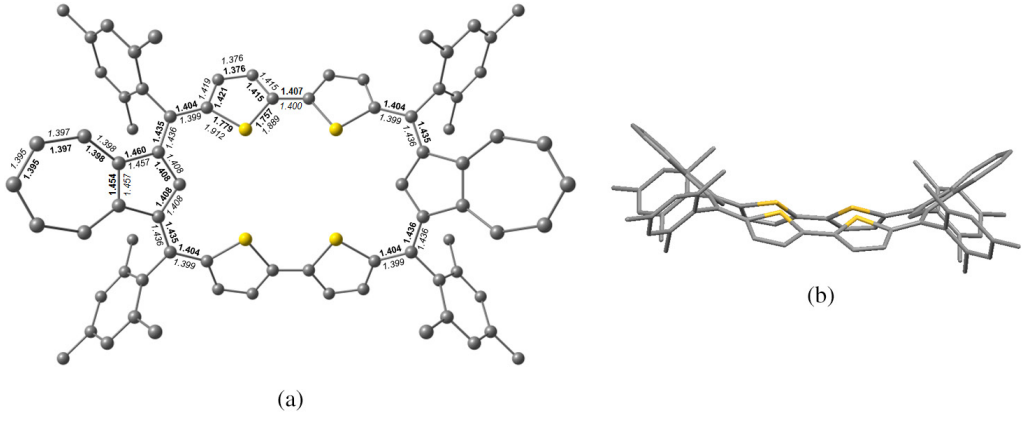

Fig. 3. DFT optimized geometries of most stable conformer of $[\mathbf{9}]^{2+}$ (a) front, (b) side view and structural parameters of optimized geometries at B3LYP/6-31G(*d*, *p*) level of theory. Note that key bond length (Å) parameters are given for $[\mathbf{9}]^{2+}$ in bold and for $[\mathbf{10}]^{2+}$ in italics. Hydrogen atoms are omitted for clarity sake

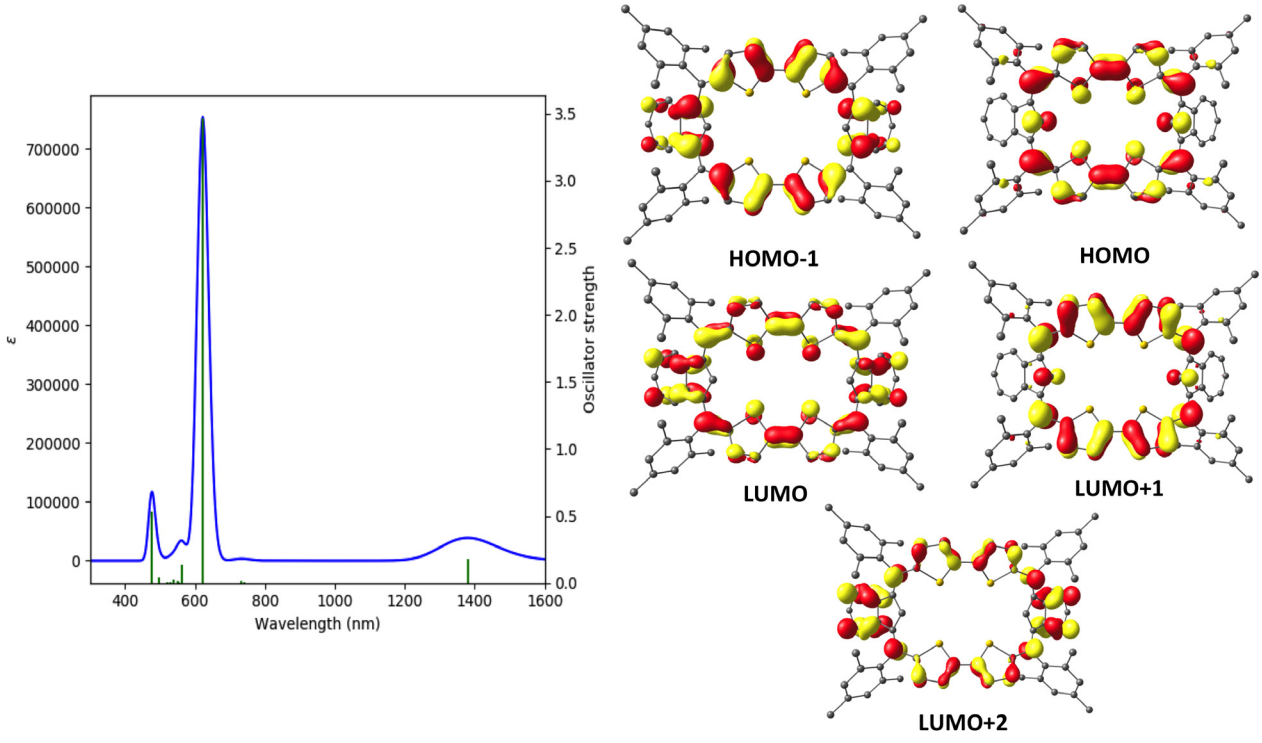

Fig. 4. TD-DFT absorption spectrum of $[\mathbf{9}]^{2+}$ and the corresponding frontier orbitals that have major contributions in electronic transitions

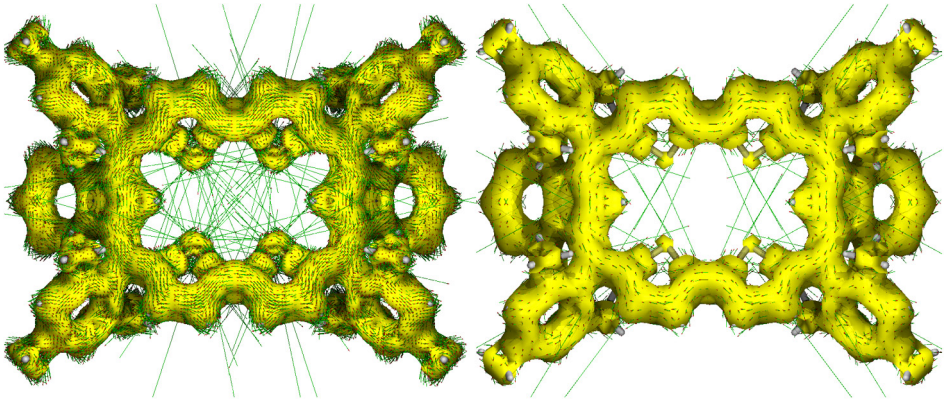

(a) (b)

Fig. 5. Anisotropy of the Induced Current Density (AICD) plot at B3LYP/6-31G (*d*, *p*) level of theory for $[\mathbf{9}]^{2+}$ (a) and $[\mathbf{10}]^{2+}$ (b)

Finally, the NMR spectrum of $[\mathbf{9}]^{2+}$ displayed characteristic features of an aromatic macrocycle in the solution state in strong support for the above-discussed theoretical results. The diatropic ring current of the macrocycle clearly distinguished the protons present in the core and on the periphery of the macrocycle. We anticipated the typical downfield resonances of the β-thiophene CH's, the tropylium character of the seven membered ring and an upfield resonance for the inner CH's of five-membered rings. The ^{1}H NMR spectral patterns upon lowering the temperature (Fig. S9) provided an insight into structural rigidity without any conceivable conformational fluxionality. At 298 K in $CDCl_3$, the ^{1}H NMR spectrum of $[\mathbf{9}]^{2+}$ exhibited sharp signals with assignable spectral features that are consistent with the most stable conformation without any heterocyclic ring inversion. In the 2D COSY spectra (Fig. 6a), the multiplet at 9.98 exhibits two sets of correlations with the broad peak at 9.22 and 9.12 ppm. In the 2D ROESY spectra (Fig. 6b), the broad peaks at 9.22 ppm and 9.12 ppm exhibit correlations with the signals at 2.09 ppm. Thus, these peaks have been unequivocally assigned as –CH

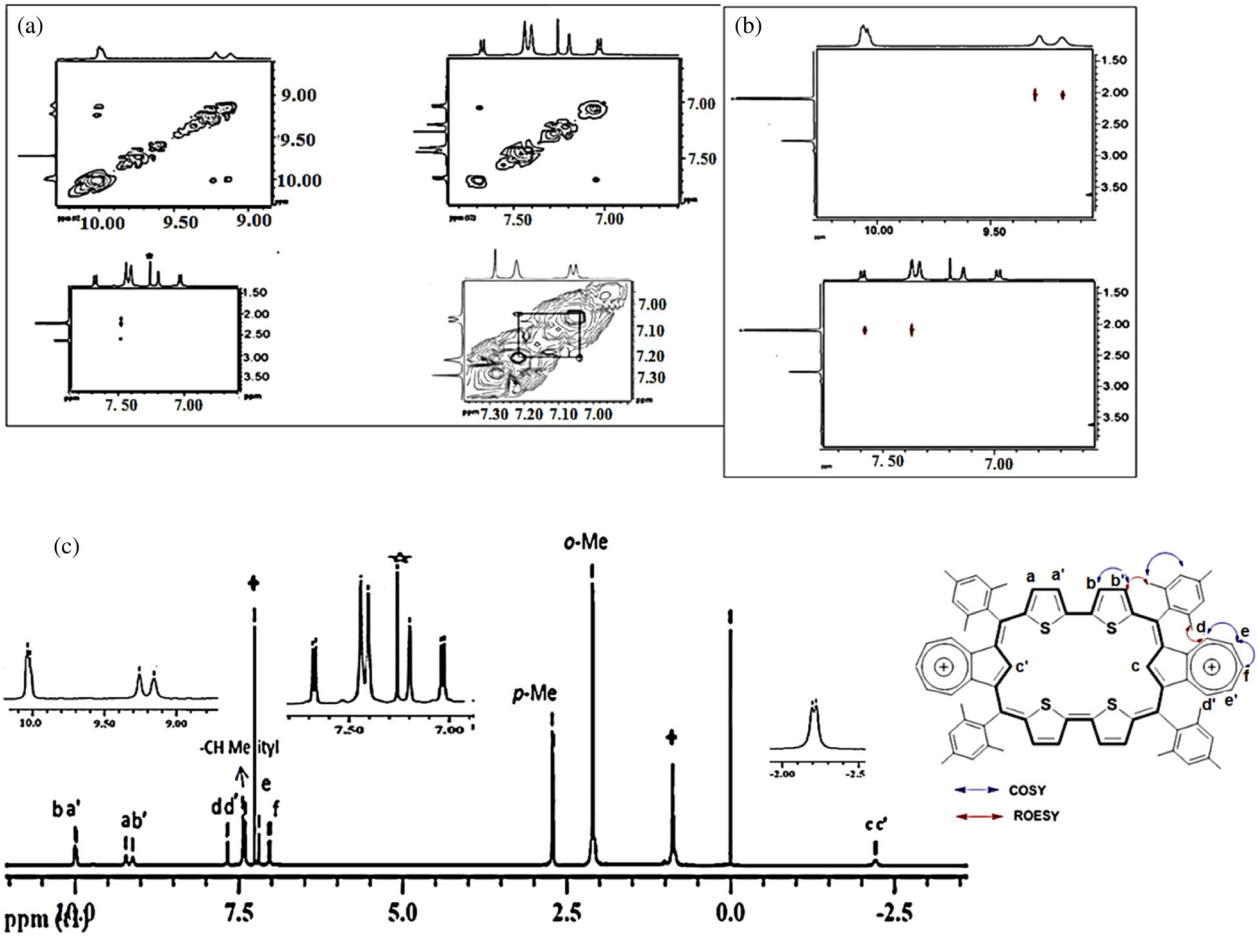

Fig. 6. ^{1}H–^{1}H 2D COSY (a), ^{1}H–^{1}H 2D ROESY (b) and Complete ^{1}H NMR spectra (c) of $[\mathbf{9}]^{2+}$ in $CDCl_3$ at 298 K

peaks (a, b′) of bithiophene rings and the later signals as *o*-Me respectively and hence accounting the multiplet at 9.98 as –CH protons a′ and b of bithiophene rings.

There are two closely spaced singlets at 7.44 and 7.40 ppm. The signal at 7.44 ppm exhibits bond correlations with an *o*-Me peak at 2.09 ppm and a *p*-Me peak at 2.70 ppm, respectively, thus accounting the former signal as *m*-CH of same mesityl ring. The singlet at 7.40 ppm exhibits bond correlations with a *p*-Me peak at 2.70 ppm, thus accounting the former signal as *m*-CH of same mesityl ring. The two well resolved doublets at 7.67 and 7.03 ppm exhibit bond correlations with each other in 2D COSY spectra, while the former doublet exhibits dipolar coupling with an *o*-Me peak at 2.09 ppm in 2D ROESY spectra, clearly revealing the former doublet as –CHs of seven-membered tropylium rings labelled as *d*, *d′* and later doublet as *e*, *e′* respectively. The two most shielded peaks at -2.19 and -2.22 ppm have been assigned as inner –CHs of five membered rings. These observations clearly reveal two types of magnetically non-equivalent tropylium units that presumably reflect a different degree of distortion from planarity in solution state, whereas both the tropylium rings are tilted inward with the mean plane deviation being 35.78° for the DFT optimized geometry of the most stable conformer of $[\mathbf{9}]^{2+}$. The decreased macrocyclic symmetry is fully supported by the magnetically nonequivalent nature of each individual proton in the macrocyclic conjugation pathway resonating separately in their respective ^{1}H NMR spectra. The calculated Δδ value from chemical shift is found to be 12.10 ppm, thus suggesting aromaticity in this macrocycle [21]. Extreme insolubility of macrocycle $[\mathbf{10}]^{2+}$ made the recording of ^{1}H NMR extraordinarily difficult. Although a definite proof from single crystal X-ray diffraction analysis is lacking at this stage for the macrocycles $[\mathbf{9}]^{2+}$ and $[\mathbf{10}]^{2+}$, DFT level analysis has clearly supported our experimental spectroscopic observations (Fig. S23).

In conclusion, the present manuscript provides conformational rigidity of two highly stable [26] dicarbaporphyrinoids. Excellent agreement between the theoretically determined properties and the experimental spectroscopic measurements are key to the evidence of strong aromaticity with NIR absorption. Our results are in accordance with the fact that inclusion of azulene moieties into macrocyclic core does not necessarily initiate borderline aromaticity. Rather, depending upon the types of macrocycles under investigation, strong aromaticity

can be induced *via* extra stable tropylium cations. Further development of such dynamic carbaporphyrinoids is currently under progress in our laboratory.

MATERIALS AND METHODS

Electronic absorption spectra were measured using a UV-vis-NIR spectrophotometer. ^{1}H, and ^{13}C NMR spectra were recorded on a spectrometers (operating at 500.13/700.13 MHz for ^{1}H and 125.77/176.05 MHz for ^{13}C) using the residual solvents as the internal references for ^{1}H ($CHCl_3$ (δ = 7.26 ppm), CH_2Cl_2 (δ = 5.32 ppm). MALDI-TOF MS data were recorded using a Bruker Daltonics Flex Analyzer and ESI HR-MS data were recorded using a Waters QTOF Micro YA263 spectrometer. All solvents and chemicals were of reagent quality, obtained commercially and used without further purification except as noted. For spectral measurements, anhydrous dichloromethane was obtained by refluxing and distillation over CaH_2. Dry THF was obtained by refluxing and distillation over pressed sodium metal. Thin layer chromatography (TLC) was carried out on alumina sheets coated with silica gel 60 F_{254} and gravity column chromatography was performed using Silica Gel 230–400 mesh.

Computational chemistry

Electronic structure calculations of core modified dicarbaporphyrinoids **9**, **10**, $[\mathbf{9}]^{2+}$ and $[\mathbf{10}]^{2+}$ were carried out using density functional theory (DFT) with Becke's three-parameter hybrid exchange functional and the Lee-Yang-Parr correlation functional (B3LYP) [16] and the 6-31G (*d*, *p*) basis set for all the atoms (B1) [17]. Further harmonic vibrational frequencies were computed on optimized geometries of all isomers to verify the nature of the stationary points. To evaluate the absorption spectra of **9**, **9**a, **10**, **10**a, $[\mathbf{9}]^{2+}$ and $[\mathbf{10}]^{2+}$, time-dependent TD-DFT calculations [22] were performed in the presence of dichloromethane using the polarizable continuum model (PCM) with the integral equation formalism variant (IEFPCM) [23] at the B1 level of theory. The effective π-electron delocalization through the system is confirmed by the NMR shielding values and the negative value of nuclear independent chemical shift (NICS) [18] calculated by using the gauge-independent atomic orbital (GIAO) [24] method based on the optimized geometries at the B1 level using tetramethylsilane as a reference standard. The magnitude and direction of the induced ring current when an external magnetic field is applied orthogonal to the macrocycle plane is displayed with AICD [19] plots by employing the continuous set of gauge transformations (CSGT) [25] method. The relative energies and Gibb's free energies of isomers **9**, $\mathbf{9}^{2+}$, **10** and $\mathbf{10}^{2+}$ were optimized at the B1 level and single point energy calculations were performed at the B3LYP/6-311+G(*d*, *p*) level of theory (B2) [26]. Note that all these calculations were carried out using the Gaussian 16 (A.03) program suite [27].

Synthesis

***5,5′-Bis-(mesitylhydroxymethyl)-2,2′-bithiophene* (6).** To a solution of *N*,*N*,*N*′,*N*′-tetramethylethylenediamine (2.7 mL, 18 mmol) in dry tetrahydrofuran (40 mL), *n*-butyllithium (11 mL, 18 mmol) was added followed by 2,2′-bithiophene (1 g, 6 mmol) under nitrogen atmosphere. The reaction mixture was stirred at room temperature for one hour and later heated under reflux for one hour. The reaction mixture was then allowed to attain 25 °C. Mesitaldehyde (2.2 mL, 15 mmol) in dry tetrahydrofuran was added dropwise to the reaction mixture at 0 °C. After addition was over, the reaction mixture was allowed to attain 25 °C. Then saturated ammonium chloride was added and it was extracted with ether or chloroform (100 mL). The organic layers were combined and washed with brine (100 mL) and dried over anhydrous sodium sulfate. The crude product obtained on evaporation was recrystallized from dry toluene, which afforded the pale solid. Yield 1.40 g (57%). mp 137 °C (decomposed). Anal. calcd. for $C_{28}H_{30}O_2S_2$: C, 72.69; H, 6.54; S, 13.86%. Found: C, 72.93; H, 6.57; S, 13.85. ^{1}H NMR (400 MHz; $CDCl_3$; Me_4Si): δ_H ppm 6.91 (d, *J* = 4Hz, 2H), 6.86 (s, 4H), 6.51 (d, *J* = 4Hz, 2H), 6.4 (s, 2H), 2.33 (s, 12H), 2.28 (s, 6H), 1.57 (brs, OH, 2H). $^{13}C\{^{1}H\}$ NMR (100 MHz; $CDCl_3$; Me_4Si): δ_C ppm 20.3, 20.8, 69.3, 122.2, 123.5, 130.0, 131.9, 135.3, 136.7, 137.8, 150.2. MS (EI): m/z 463.1757 (calcd. for $[M + H]^+$).

***5,5′-Bis-(mesitylhydroxymethyl)-2,2′-biselenophene* (7).** A similar procedure as mentioned above was followed with biselenophene (1 g, 3.8 mmol), *n*-butyllithium (7.5 mL, 11.4 mmol) and mesitaldehyde (1.4 mL, 9.5 mmol) to obtain **7**. The crude product was precipitated out by hexane and purified by silica gel column chromatography using the mixture of ethyl acetate — hexane (20:80) solution. The solvent was evaporated and a light yellow solid was obtained. Yield 1.50 g (67%). mp 137 °C (decomposed). Anal. calcd. for $C_{28}H_{30}O_2Se_2$: C, 60.44; H, 5.43; Se, 28.38%. Found: C, 60.95; H, 5.57. ^{1}H NMR (400 MHz; $CDCl_3$; Me_4Si): δ_H ppm 6.9 (d, *J* = 3.96 Hz, 2H), 6.78 (s, 4H), 6.5 (m, 2H), 6.29 (s, 2H), 2.27 (s, 12H), 2.2 (s, 6H). $^{13}C\{^{1}H\}$ NMR (100 MHz; $CDCl_3$; Me_4Si): δ_C ppm 20.6, 29.8, 69.8, 124.7, 126.3, 130.2, 135.3, 137.0, 137.9, 138.3, 148.8. MS (EI): m/z 579.0054 (calcd. for $[M^+ + Na]^+$).

***Compound* $[\mathbf{9}]^{2+}$.** Under nitrogen atmosphere and in dark conditions, a solution of compound **6** (462 mg, 1 mmol) and azulene (128 mg, 1 mmol) in 250 mL dry dichloromethane was stirred for 30 min. Afterward, a catalytic amount of $BF_3 \cdot Et_2O$ (0.1 mL) was added to the reaction mixture and stirred at room temperature for 90 min. Then chloranil (614 mg, 2.5 mmol) was added and opened to air and the mixture was refluxed for another 1 h. The solvent was removed under reduced

pressure and compound was filtered on basic alumina followed by repeated silica gel column chromatography with a mixture of 1% methanol — dichloromethane solution. After recrystallization, the title compound was yielded as dark green solids. Yield. ~101mg. mp 300 °C (decomposed). Anal. calcd. for $C_{76}H_{64}S_4$: C, 82.57; H, 5.84; S, 11.60%. Found: C, 82.97; H, 5.97; S, 11.06. ^{1}H NMR (500 MHz; $CDCl_3$; Me_4Si): δ_H ppm -2.19 (s, 1H, CH); -2.22 (s, 1H, CH); 2.09 (s, 24H, *o*-CH_3); 2.70 (s, 12H, *p*-CH_3); 7.03 (m, 4H, -CH tropylium); 7.25 (brs, 2H, -CH tropylium); 7.40 (s, 4H, -CH mesityl); 7.44 (s, 4H, -CH mesityl); 7.67 (m, 4H, -CH tropylium); 9.12 (d, J = 4.2 Hz, 2H, thiophene β-H); 9.22 (d, J = 4.2 Hz, 2H, thiophene β-H); 9.98 (m, 4H, thiophene β-H). UV-vis (ϵ [$M^{-1} \cdot cm^{-1} \times 10^5$]): λ, nm, 587 (4.5), 702 (0.81), 788 (0.86), 1305 (0.29). MS (MALDI-TOF): (m/z) 1104.279 (calcd. for $[M]^+$).

***Compound* $[10]^{2+}$.** Under nitrogen atmosphere and in dark conditions, a solution of compound **7** (556 mg, 1 mmol) and azulene (128 mg, 1 mmol) in 250 mL dry dichloromethane was stirred for 30 min. Afterward, a catalytic amount of $BF_3 \cdot Et_2O$ (0.1 mL) was added to the reaction mixture and stirred at room temperature for 90 min. Then chloranil (614 mg, 2.5 mmol) was added and opened to air and the mixture was refluxed for another 1 h. The solvent was removed under reduced pressure and the compound was filtered by basic alumina followed by repeated silica gel column chromatography with the a mixture of 1% methanol — dichloromethane solution. After recrystallization, the title compound was yielded as dark green solids. Yield. ~101mg. mp 300 °C (decomposed). Anal. calcd. for $C_{76}H_{64}Se_4$: C, 70.59; H, 4.99; Se, 24.42%. Found: C, 70.98; H, 5.01. UV-vis (ϵ [$M^{-1} \cdot cm^{-1} \times 10^5$]): λ, nm, 620 (4.5), 735 (0.91), 802 (0.96), 1385 (0.32). MS (MALDI-TOF): (m/z) 1296.451(calcd. for $[M]^+$).

Acknowledgments

KCS thanks CSIR, New Delhi for senior research fellowship. HR thanks DST-SERB (EMR/2016/004705), New Delhi, India for research grant. MS thanks CFTRI for research fellowship. DU thanks CFTRI for computing facilities.

Supporting information

MS spectra, ^{1}H and ^{13}C NMR spectra of precursors, Low VT NMR spectra, theoretical data and X, Y, Z coordinates are given in the supplementary material. This material is available free of charge *via* the Internet at http://www.worldscinet.com/jpp/jpp.shtml.

REFERENCES

1. (a) Won D-II, Lee J-S, Ba Q, Cho Y-J, Cheong H-Y, Choi S, Kim CH, Son H-J, Pac C and Kang SO. *ACS Catal.* 2018; **8**: 1018–1030. (b) Ding Y, Zhu W-H and Xie Y. *Chem. Rev.* 2017; **117**: 2203–2256. (c) Schmitt F, Govindaswamy P, Süss-Fink G, Ang WH, Dyson PJ, Juillerat-Jeanneret J and Therrien B. *J. Med. Chem.* 2008; **51**: 1811–1816. (d) Tanaka H, Ikeda T, Takeuchi M, Sada K, Shinkai S and Kawai T. *ACS. Nano* 2011; **5**: 9575–9582. (e) Gryko DT, Clausen C, Roth KM, Dontha N, Bocian DF, Kuhr WG and Lindsey JS. *J. Org. Chem.* 2000; **65**: 7345–7355.
2. (a) Waignright M. *Color. Technol*. 2010; **126**: 115–126. (b) Pawlicki M, Collins HA, Denning RG and Anderson HL. *Angew. Chem., Int. Ed*. 2009; **48**: 3244–3266. (c) Carr JA, Franke D, Caram JR, Perkinson CF, Saif M, Askoxylakis V, Datta M, Fukumura D, Jain RK, Bawendi MG and Bruns OT. *Proc. Natl. Acad. Sci*. USA. 2018; **115**: 4465–4470 and references therein.
3. Sahoo KC, Kumaraswami M, Usharani D and Rath H. *J. Org. Chem*. 2019; **84**: 5203–5212.
4. (a) Rath H, Mallick A, Ghosh T and Kalita A. *Chem. Commun*. 2014; **50**: 9094–9096. (b) Mallick A, Oh J, Kim D and Rath H. *Chem. — Eur. J.* 2016; **22**: 8026–8031. (c) Shin J-Y, Furuta H and Osuka A. *Angew. Chem., Int. Ed.* 2001; **40**: 619–621. (d) Lash TD. *J. Porphyrins Phthalocyanines*. 2001; **5**: 267–288. (e) Panda PK, Kang Y-J and Lee C-H. *Angew. Chem., Int. Ed*. 2005; **44**: 4053–4055. (f) Wu D, Descalzo AB, Emmerling F, Shen Z and You X-Z. *Angew. Chem., Int. Ed.* 2008; **47**: 193–197. (g) Chang Y, Chen H, Zhou Z, Zhang Y, Schutt C, Herges R and Shen Z. *Angew. Chem., Int. Ed.* 2012; **51**:12801–12805. (i) Anguera G, Cha W-Y, Moore MD, Brewster II JT, Zhao MY, Lynch VD, Kim D and Sessler JL. *Angew. Chem., Int. Ed.* 2018; **57**: 2575–2579.
5. Mori H, Tanaka T and Osuka A. *J. Mat. Chem. C* 2013; **1**: 2500–2519, and references therein.
6. Lash TD. *Chem. Rev.* 2017; **117**: 2313–2441.
7. (a) Berlicka A, Dutka P, Szterenberg L and Latos-Grażyński L. *Angew. Chem., Int. Ed*. 2014; **53**: 4885−4889. (b) Lash TD. *Eur. J. Org. Chem*. 2007; 5461−5481. (c) Pawlicki M and Latos-Grażyński L. *Chem. Rec.* 2006; **6**: 64−78. (d) Szterenberg L and Latos-Grażyński L. *Inorg. Chem*. 1997; **36**: 6287−6291. (e) Chemielewski PJ, Latos-Grażyński L and Glowiak T. *J. Am. Chem. Soc.* 1996; **118**: 5690−5701. (f) Chmielewski PJ, Latos-Grażyński L and Schmidt I. *Inorg.* Chem. 2000; **39**: 5475−5482. (g) Furuta H, Ogawa T, Uwatoko Y and Araki K. *Inorg. Chem.* 1999; **38**: 2676−2682. (h) Furuta H, Kubo N, Ishizuka T, Osuka A, Nanami H and Ogawa T. *Inorg. Chem*. 2000; **39**: 5424−5425. (i) Ogawa T, Furuta H, Takahashi M, Morino A and Uno H. J. *Organomet. Chem*. 2000; **611**: 551−557. (j) Furuta H, Maeda H, Osuka A, Yasutaka M, Shinmyozu T and Ishikawa Y. *Chem. Commun*. 2000; 1143−1144.

8. (a) Lash TD, Colby DA and Szczepura LF. *Inorg. Chem.* 2004; **43**: 5258–5267. (b) Adiraju VAK, Ferrence GM and Lash TD. *Dalton Trans*. 2016; **45**: 13691–13694.
9. Lash TD. *Eur. J. Org. Chem*. 2007; 5461–5481.
10. Lash TD. *Acc. Chem. Res*. 2016; **49**: 471–482.
11. Lash TD, El-Beck JA and Ferrence GM. *Org. Biomol. Chem*. 2014; **12**: 316–329 and references therein.
12. (a) Sprutta N, Swiderska MSÄ and Latos-Grażyński L. *J. Am. Chem. Soc*. 2005; **127**: 13108–13109. (b) Sprutta N, Siczek M, Latos-Grażyński L, Szterenberg L and Lis T. *J. Org. Chem*. 2007; **72**: 9501–9509.
13. (a) Lash TD, Colby DA, Graham SR, Ferrence GM and Szczepura LF. *Inorg. Chem*. 2003; **42**: 7326–7337. (b) Lash TD. *Chem. — Asian J*. 2014; **9**: 682–705.
14. (a) Chandrashekar TK and Misra R. *Acc. Chem. Res.* 2008; **41**: 265–279. (b) Chandrashekar TK and Venkataraman S. *Acc. Chem. Res.* 2003; **36**: 676–691. (c) Srinivasan A, Reddy VRM, Narayanan SJ, Sridevi B, Pushpan SK, Ravikumar M and Chandrashekar TK. *Angew. Chem., Int. Ed.* 1997; **36**: 2598–2601.
15. Gouterman M. *J. Mol. Spectrosc.* 1963; **11**: 108–127.
16. (a) Becke ADJ. *J. Chem. Phys*. 1993; **98**: 1372–1377. (b) Lee C, Yang W and Parr RG. *Phys. Rev. B* 1988; **37**: 785–789.
17. (a) Petersson GA, Bennett A, Tensfeldt TG, Al-Laham MA, Shirley W and Mantzaris AJ. *J. Chem. Phys*. 1988; **89**: 2193–2218. (b) Petersson GA and Al-Laham MA. *J. Chem. Phys*. 1991; **94**: 6081–6090.
18. Schleyer PVR, Maerker C, Dransfeld A, Jiao H and Hommea NJRVE. *J. Am. Chem. Soc*. 1996; **118**: 6317–6318.
19. Geuenich D, Hess K, Köhler F and Herges R. *Chem. Rev*. 2005; **105**: 3758–3772.
20. (a) Krygowski TM *J. Chem. Inf. Comut. Sci*. 1993; **33**: 77–78. (b) Krygowski TM and Cryański KM. *Chem. Rev*. 2001; **101**: 1385–1420.
21. Franck B and Nonn A. *Angew. Chem., Int. Ed.* 1995; **34**: 1795–1811.
22. (a) Scalmani G, Frisch MJ, Mennucci B, Tomasi J, Cammi R and Barone V. *J. Chem. Phys.* 2006; **124**: 094107/1– 094107/15. (b) Adamo C and Jacquemin D. *Chem. Soc. Rev*. 2013; **42**: 845–856. (c) Miertuš S and Tomasi J. *J. Chem. Phys*. 1982; **65**: 239–245. (d) Cossi M and Barone V. *J. Chem. Phys*. 2000; **112**: 2427–2735.
23. (a) Miertuš S and Tomasi J. *J. Chem. Phys.* 1982; **65**: 239–245. (b) Cossi M and Barone V. *J. Chem. Phys.* 2000; **112**: 2427–2435.
24. (a) Wolinski K, Hilton JF and Pulay P. *J. Am. Chem. Soc.* 1990; **112**: 8251–8260. (b) London FJ. *Phys. Radium*. 1937; **8**: 397–409.
25. (a) Cheeseman JR, Trucks GW, Keith TA and Frisch MJ. *J. Chem. Phys.* 1996; **104**: 5497–5509. (b) Keith TA and Bader RFW. *Chem. Phys. Lett*. 1993; **210**: 223–231.
26. (a) Wachters AJH. *J. Chem. Phys.* 1970; **52**: 1033–1036. (b) Hay PJ. *J. Chem. Phys.* 1977; **66**: 4377–4384.
27. Gaussian 16, Revision A.03, Frisch MJ, Trucks GW, Schlegel HB, Scuseria GE, Robb MA, Cheeseman JR, Scalmani G, Barone V, Petersson GA, Nakatsuji H, Li X, Caricato M, Marenich AV, Bloino J, Janesko BG, Gomperts R, Mennucci B, Hratchian HP, Ortiz JV, Izmaylov AF, Sonnenberg JL, Williams-Young D, Ding F, Lipparini F, Egidi F, Goings J, Peng B, Petrone A, Henderson T, Ranasinghe D, Zakrzewski VG, Gao J, Rega N, Zheng G, Liang W, Hada M, Ehara M, Toyota K, Fukuda R, Hasegawa J, Ishida M, Nakajima T, Honda Y, Kitao O, Nakai H, Vreven T, Throssell K, Montgomery JA Jr., Peralta JE, Ogliaro F, Bearpark MJ, Heyd JJ, Brothers EN, Kudin KN, Staroverov VN, Keith TA, Kobayashi R, Normand J, Raghavachari K, Rendell AP, Burant JC, Iyengar SS, Tomasi J, Cossi M, Millam JM, Klene M, Adamo C, Cammi R, Ochterski JW, Martin RL, Morokuma K, Farkas O, Foresman JB and Fox DJ. Gaussian, Inc., Wallingford CT, **2016**.